Macromolecular Research, Vol. 15, No. 6, pp 565-574 (2007)

Gas Separation of Pyrolyzed Polymeric Membranes: Effect of Polymer Precursor and Pyrolysis Conditions

Chul Ho Jung, Gun Wook Kim, Sang Hoon Han, and Young Moo Lee*

School of Chemical Engineering, College of Engineering, Hanyang University, Seoul 133-791, Korea

Received June 1, 2007; Revised July 31, 2007

Abstract: In this study, five representative, commercially available polymers, Ultem 1000 polyetherimide, Kapton polyimide, phenolic resin, polyacrylonitrile and cellulose acetate, were used to prepare pyrolyzed polymer membranes coated on a porous α-alumina tube via inert pyrolysis for gas separation. Pyrolysis conditions (i.e., final temperature and thermal dwell time) of each polymer were determined using a thermogravimetric method coupled with real-time mass spectroscopy. The surface area and pore size distribution of the pyrolyzed materials derived from the polymers were estimated from the nitrogen adsorption/desorption isotherms. Pyrolyzed membranes from polymer precursors exhibited type I sorption behavior except cellulose acetate (type IV). The gas permeation of the carbon/α-alumina tubular membranes was characterized using four gases: helium, carbon dioxide, oxygen and nitrogen. The polyetherimide, polyimide, and phenolic resin pyrolyzed polymer membranes showed typical molecular sieving gas permeation behavior, while membranes from polyacrylonitrile and cellulose acetate exhibited intermediate behavior between Knudsen diffusion and molecular sieving. Pyrolyzed membranes with molecular sieving behavior (e.g., polyetherimide, polyimide, and phenolic resin) had a CO_2/N_2 selectivity of greater than 15; however, the membranes from polyacrylonitrile and cellulose acetate with intermediate gas transport behavior had a selectivity slightly greater than unity due to their large pore size.

Keywords: gas separation, polyimide, phenolic resin, polyacrylonitrile, cellulose acetate, pyrolized membrane.

Introduction

Pyrolyzed polymers have received much attention for various applications such as gas separation, purification, and storage.[1] Compared to polymeric membranes, pyrolyzed polymer membranes (PPM) and carbon molecular sieve membranes (CMSM) have shown advantages in high gas permeability and permselectivity due to their excellent shape selectivity for planar molecules, high hydrophobicity, heat resistance and high corrosion resistance.[2-4]

Thermosetting polymers have been used for preparing PPM or CMSM suitable for gas separations after pyrolysis.[5,6] It is often difficult to produce a high performance carbon membrane due to many steps which must be precisely controlled and optimized. In addition, module configuration among flat-sheet, hollow fiber, and support types are also important factors to consider due to handling problems of the brittle carbon materials. A typical fabrication process of PPMs includes the selection of a precursor, preparation of the polymeric membrane, pre-treatment, pyrolysis/carbonization, post-treatment, and module construction.[7] In this process, the pyrolysis step, including pretreatment, and the selection of polymer precursor are the most important steps influencing the final properties of PPM. Preparation conditions for various thermoset polymers were previously summarized according to pyrolysis conditions and configuration.[4] Previous investigations have focused mainly on the change in PPM separation performance and microstructure by controlling pyrolysis conditions such as pyrolysis temperature, carbonization environment, heating rate, and soaking time.[5,8-13] Specifically, many researchers have concentrated on the PPM performance related to the external environments of selected polymeric precursors. Although consideration of the thermal stability of the polymeric precursor is a key factor controlling the pyrolysis temperature, no systematic studies have been performed.

Several polymeric precursors have been tested to prepare composite type membrane modules as shown in Table I. PPM from polyimide precursor showed relatively higher gas separation performance than that from other polymer precursors due to their excellent shape selectivity. Selection of the polymer precursor is an important factor to prepare PPM composite membranes and modules. A fair comparison of PPM composite membrane modules with the same

*Corresponding Author. E-mail: ymlee@hanyang.ac.kr

Table I. Summary of Ceramic Supported Type PPM Membranes Prepared and Characterized by Different Investigators

Polymeric Precursor		Pyrolysis temp (°C)	CO_2 Permeance (GPU)	Separation Factor	Ref
Polyimide	(BPDA-pp'ODA)	800 (N_2)	~6	$CO_2/CH_4 \approx 100$ $CO_2/N_2 \approx 27$	28
Polyimide	(BPDA-pp'ODA)	700 (Ar)	~90	$CO_2/N_2 \approx 40$	29
Polyimide	(BPDA-ODA/DAT)	700 (oxidation at 400 °C)	~300	$CO_2/CH_4 \approx 15$	30
Polyimide	(Kapton)	600	~1200	$CO_2/N_2 \approx 12$	31
Polyetherimide	(Ultem 1000)	600 (Ar)	~290	$CO_2/CH_4 \approx 60$	21
Phenolic resin		700 (vacuum)	~80	$CO_2/CH_4 \approx 10$ $CO_2/N_2 \approx 6$	9
Phenol formaldehyde		900	~0.6	$CO_2/CH_4 \approx 21$ $CO_2/N_2 \approx 9$	32
Sulfonated phenolic resin		500	0.3~800	$CO_2/CH_4 = 4$~27	33

thickness and the optimum pyrolysis temperature was difficult to achieve due to many variables during the preparation process, such as coating, pyrolysis and module preparation. However, it remains significant to understand the correlation between pore structure and gas permeation performance using the same conditions to determine the transport mechanisms of different PPM modules prepared from various polymeric precursors.

To this end, PPM modules were fabricated with five representative commercial polymers using pyrolysis conditions tailored to each precursor. The correlation between the gas permeation properties of the PPM and structural characteristics of the precursors were studied at precisely controlled conditions by dip-coating an α-alumina tube.

Experimental

Materials. Poly(amic acid), a prepolymer of polyimide (PI), polyacrylonitrile (PAN) and cellulose acetate (CA) were purchased from Aldrich Chemical (Milwaukee, WI, USA). Phenolic resin (Novolak type, PHE) was donated from Kangnam Chemical (Ansan, Gyeonggi-do, Korea). Polyetherimide (Ultem 1000, PEI) was obtained from GE plastics (Pittsfield, MA, USA). An α-alumina tube (Nano Pore Materials Co., Seoul, Korea, porosity: 35%, pore size: 5-50 nm, O.D. 8 mm, I.D. 7 mm, length 30 mm) was used as a support.

Preparation of Pyrolyzed Polymer Composite Membranes. Pyrolyzed polymer/α-alumina composite membranes were fabricated by conventional dip-coating of the polymeric precursor solution such that the substrate was immersed in each polymer solution and retracted with a well-defined speed (2 cm/min) under controlled temperature (25 °C) and humidity (RH = 20%). The coating thickness was primarily varied by the withdrawal speed, solid content and viscosity of the polymer solution. When the withdrawal speed maintains shear rates within Newtonian behavior, the coating thickness can be calculated by the Landau-Levich eq. (1):

$$h_\infty = 0.94 \frac{(\eta \cdot U)^{2/3}}{\gamma_{LV}^{1/6} \cdot (\rho \cdot g)^{1/2}} \quad (1)$$

where h_∞ is the equilibrium thickness, η is the viscosity of coating solution, U is the withdrawal speed, ρ is the density, γ_{LV} is the liquid-vapor surface tension and g is the acceleration due to gravity. From eq. (1), the coated thickness was mainly affected by the solution viscosity when the withdrawal speed and precursor density was constant. Therefore, to maintain the same coating conditions, the viscosity of the precursor solutions was precisely controlled using a viscometer (Brookfield DV-II+ Pro, MA, USA). To produce an optimum polymer thickness of approximately 10 μm, the target viscosity of each polymer solution varied between 185-200 P (Poise). For this purpose, the solution concentration was adjusted to match the target viscosity as follows: CA (8 wt%), PHE (35 wt%), and PEI (10 wt%) dissolved in NMP and PAN (8 wt%) dissolved in DMF. Poly(amic acid) was diluted to 10 wt% using NMP. Each polymer precursor solution was dip-coated five times on the α-alumina tube to prevent crack or pin-hole formation. CA was dip-coated ten times due to the lowest thermal stability, which might be explained in detail by the TGA results. After dip-coating process, the solvent was evaporated at 60 °C for 48 h using a convective oven. After solvent evaporation, an approximately 10-μm thick polymer layer was coated on the α-alumina support. The pyrolysis procedure with a muffled furnace is shown in Figure 1[14] and was selected according to the thermal degradation history of the precursor and residual weight from a TGA-MS thermogram as shown in Figure 2. For example, the final pyrolysis temperature was determined from the weight derivative of the degradation temperature of the TGA-MS thermogram. To imidize poly(amic acid) prior to pyrolysis, a thermal imidization process was performed under vacuum at 350 °C for 1 h.

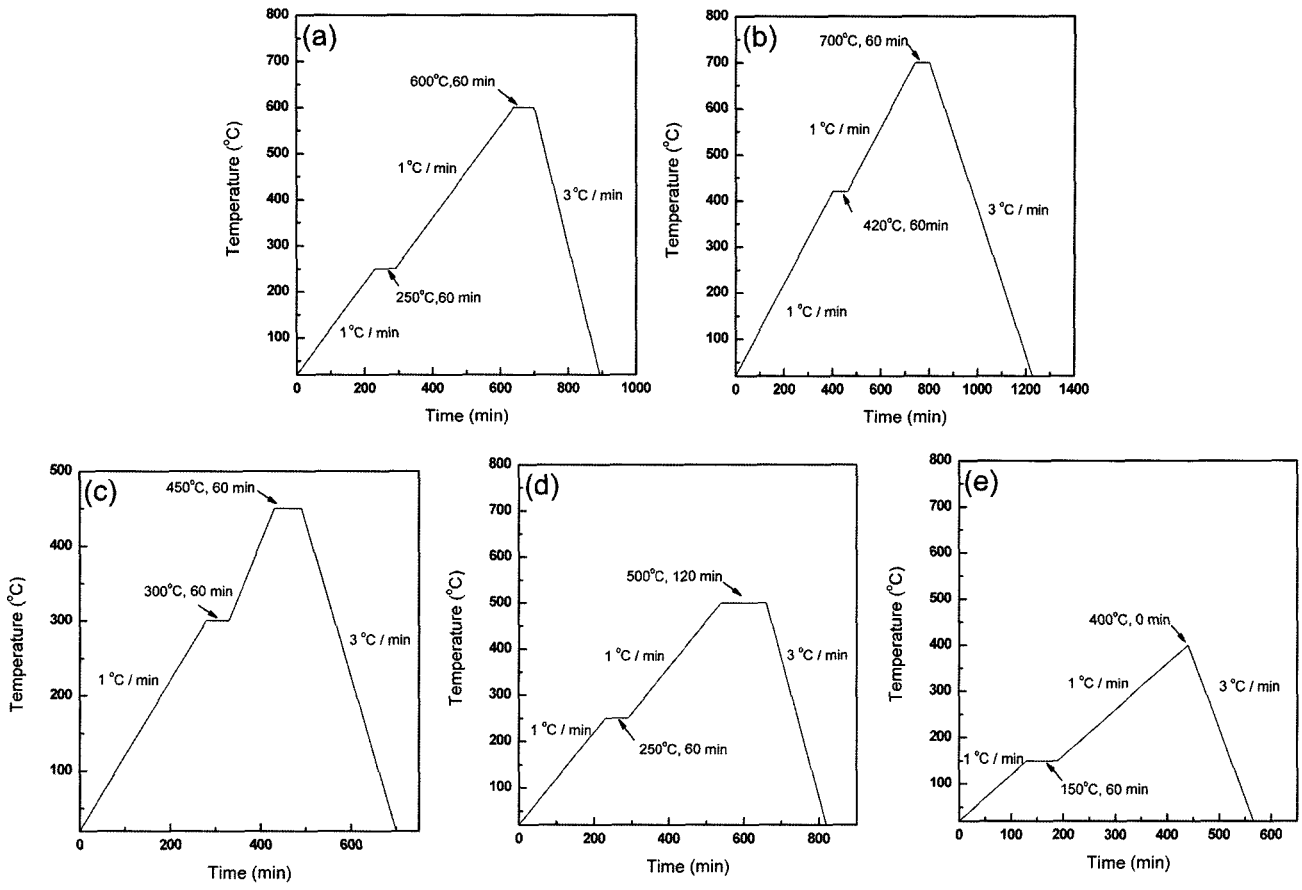

Figure 1. Pyrolysis steps of (a) PEI, (b) PI, (c) PHE, (d) PAN, and (e) CA polymer precursors (ascending rate 1 °C/ min, descending rate 3 °C/ min).

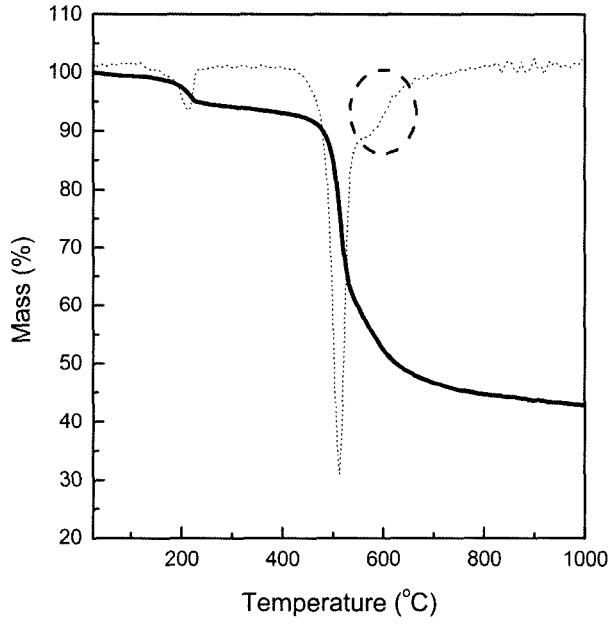

Figure 2. Typical TGA thermogram of PEI polymeric precursors.

Membrane Module Preparation. Pyrolyzed polymer/α-alumina composite membranes were carefully placed in a stainless-steel membrane module end-capped with a silicone O-ring and sealed by screw-type joint nuts, as shown in Figure 3. In order to prevent crack or scratch formation, the ends of the carbon membrane module were sealed with 5-cm long Teflon tape. The effective membrane length and area was approximately 20 cm and 100 cm^2, respectively. The module can withstand up to 200 °C, no special sealant was required to seal the ceramic support and coating layer, and the modules were easily reused in high temperature permeation experiments.

Characterization. TGA was performed using a TG209F1 (NETZSCH, Germany) with an inert atmosphere (Ar flow) from 25-1000 °C and a heating rate of 10 °C/min to confirm the thermal properties and carbonization temperature of each polymer precursor. Mass spectroscopy was used to measure the emission of various gases such as CO_2, H_2, CH_4, H_2O, and CO during pyrolysis. FT-IR spectra of the polymeric precursors and carbonized polymers were measured using a Nicolet Magna IR 760 spectrometer (Thermo Nicolet, Waltham, MA) operating in a wavenumber range of 400-4000 cm^1. X-ray diffraction patterns of polymeric pre-

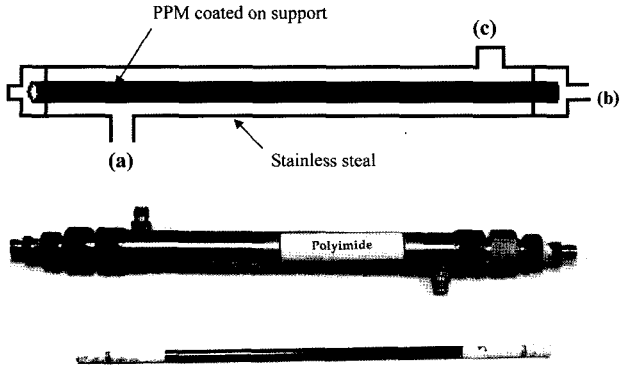

Figure 3. The (a) feed, (b) permeate, and (c) retentate of the carbon composite membrane module.

cursors and pyrolyzed materials were measured using a wide-angle X-ray diffractometer (D/MAX-2500, Rigaku, Japan) operating in the 2-theta range of 5-60° with a scan rate of 5°/min. N_2 adsorption and desorption, and pore size distribution of the PPM were measured using a surface area and porosimetry analyzer (ASAP2020, Micrometrics, GA, USA) to categorize and characterize pore characteristics of the amorphous carbon structures. Additionally, the morphology of the fabricated PPM was measured using a field emission scanning electron microscope (JSM-6330F, JEOL, Japan).

Gas Permeability Test. In order to analyze the permeation characteristics of the membrane module, the single gas permeance of the PPM fabricated from the polymeric precursors was measured according to the pressure ratio and temperatures. As shown in Figure 3, pure gases (He, O_2, N_2, and CO_2) entered in the feed side of the module (a) at an operating pressure ratio between 1-6 atm using a pressure gauge located at the retentate (c). The permeate side (b) gas flow was measured using a mass flow controller (MKS Instruments, MA, USA) at a predetermined pressure ratio between 298-393 K. Single gas permeance was obtained from the average value measured at each pressure ratio with dead-end conditions (stage cut = 1, Stage cut is defined to be the ratio of the permeate to feed flow rates). The single gas permeance P (GPU = 1×10^{-6} cm^3 (STP)/cm^2·sec·chHg), which is defined as the flux normalized by pressure and membrane area, can be calculated as:

$$P = \frac{Flux}{Area \times pressure} \quad (2)$$

The ideal permselectivities of two gas pairs (O_2/N_2 and CO_2/N_2) were calculated from the ratio of single gas permeance for the PPMs.

Results and Discussion

Morphological Changes During Pyrolysis. Thermal properties of the polymeric precursors are vital factors to determine final microstructures and gas permeation properties of their pyrolyzed membranes. A typical TGA thermogram of the PEI polymeric precursor is shown in Figure 2. The pyrolysis temperature for each polymeric precursor was selected as the endpoint of the weight loss derivative in the TGA-MS thermogram. The final pyrolysis temperature of each polymeric precursor was selected as follows: PEI (600 °C), PI (700 °C), PHE (450 °C), PAN (500 °C), and CA (400 °C). The weight residue at each pyrolysis temperature was approximately 50-65%, except for CA, which showed the steepest weight loss between 300-400 °C with 25% weight residue. For CA, the coating layer thickness was nearly half of the other precursors. To this end, the CA dip-coating process was doubled to compensate for the thin coating layer after weight loss.

Structural changes during pyrolysis were observed using FT-IR spectroscopy, as shown in a typical PAN spectra in Figure 4. The characteristic peaks of the commercial polymers before pyrolysis were represented by FT-IR spectra,[15] however, after pyrolysis, the characteristic peaks of the five polymer precursors transformed to a broad halo spectra below 1700 cm^{-1}. The transformed peak shapes were nearly the same for all the precursors. Mariwala and Foley reported that a highly chaotic structure of amorphous carbon and very small aromatic microdomains are formed during pyrolysis at these temperatures (400-700 °C).[16] To this end, the polymer structures transformed to amorphous carbon structures.

David and Ismail reported that PAN can be transformed

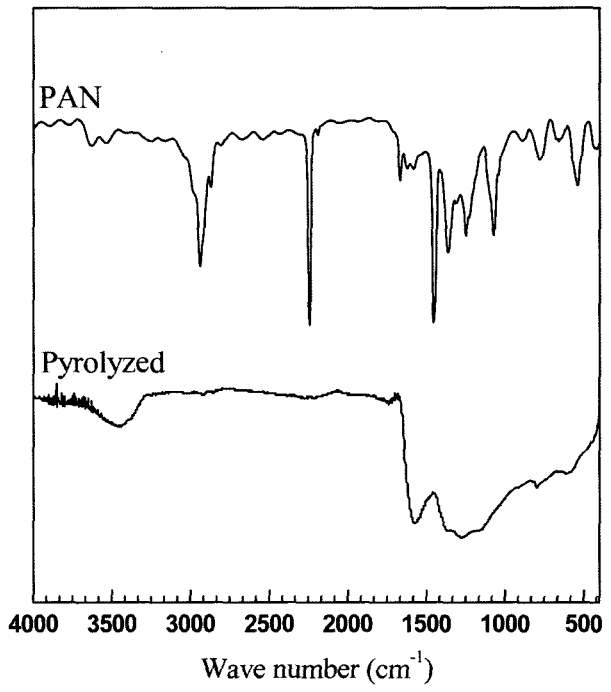

Figure 4. Typical FT-IR spectra of PAN before and after pyrolysis.

Table II. Average d-Spacing of Precursor and Pyrolyzed Polymers from WAXD

	d-Spacing (Å)	
	Virgin polymer precursor	Pyrolyzed polymer
PEI	5.83	3.58
PI	5.10	4.44
PHE	4.08	3.79
PAN	5.11	3.78
CA	5.24	3.74

into heterocyclic structures during an inert or oxidative stabilization process.[17] Similarly, Grzyb *et al.* characterized the transformation of the PAN structure according to thermal history. The PAN precursor undergoes non-aromatic cyclic tautomeric structure between polyimide and polyenamine to form an aromatic carbon structure.[18] After pyrolysis at 500 °C, a broad band from the aromatic ring (1600 cm^{-1}) and nitrogen functionalities (3100-3500 cm^{-1} and 1200-1400 cm^{-1}) arose due to pyrolysis of the PAN precursor. Aromatization is also reflected by disappearance of the aliphatic C-H band at 2800-3000 cm^{-1}.[19] As shown in Figure 4, the PPM spectra obtained from the PAN precursor corroborated these analyses.

The structural characteristics of the carbon membranes were determined from X-ray diffraction. Additionally, WAXD data are useful for determining the interplanar distance in the PPMs from the maximum intensity in the amorphous scattering, which gives a broad band indicating a *d*-space distribution.[20] Average *d*-spacing values of each of the polymeric precursors and corresponding PPMs are summarized in Table II. The *d*-spacing values (interlayer distance) of all polymer precursors decreased after carbonization, indicating that the polymers transformed to a denser structure. The *d*-spacing values of the PPMs varied between 3.6-3.8 Å, except the PPM from PI (4.4 Å). A wider *d*-spacing can act as a positive path for gas permeability. From the FT-IR spectra and X-ray diffraction patterns, it was confirmed that polymeric precursors transformed to a wholly amorphous carbon structure with small *d*-spacing.

Effect of Polymer Precursors on Pore Characteristics. Gas adsorption experiments in meso- and microporous regions provide useful information regarding the structure of the carbon membrane.[21] To study the adsorption process of the PPMs derived from various polymeric precursors, the isothermal N_2 adsorption and desorption isotherms were studied using the Brunauer-Emmett-Teller (BET) method,

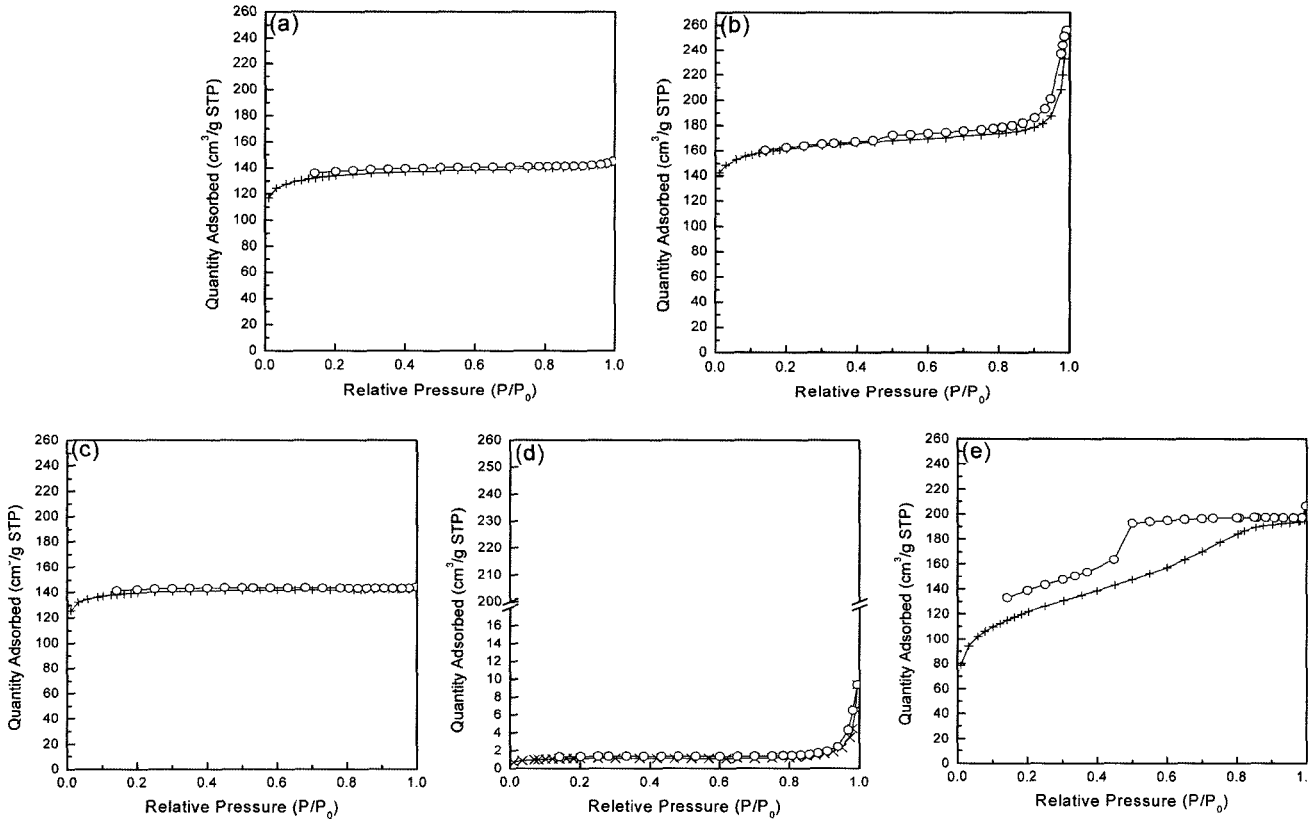

Figure 5. Isothermal adsorption and desorption of pyrolyzed polymer membrane rendered from (a) PEI, (b) PI, (c) PHE, (d) PAN, and (e) CA.

Table III. Characterization of N_2 Isotherms and Pores after Pyrolyzing Membranes Rendered from Five Polymer Precursors

Polymer Type	IUPAC Classification	Surface Area (m^2/g) (at $P/P_0 = 0.2$)	Pore Volume (cm^3/g) (at $P/P_0 = 0.97$)	Average Pore Size (Å)
PEI	Type I	465	0.22	19.6
PI	Type I	560	0.32	23.7
PHE	Type I	485	0.22	18.9
PAN	Type I	4	0.006	55.2
CA	Type IV	423	0.30	28.1

as shown in Figure 5. According to IUPAC classification, the isotherm shapes can be classified into six major categories. Adsorption isotherms of tested PPMs were classified as shown in Table III. The adsorption isotherms of tested PPM membranes showed type I behavior except CA. The type I isotherm of adsorption may show an abrupt increase in the low pressure region, which implies the existence of abundant microporous carbon structures and no mesopores.[22] However, the PPM formed from CA exhibited a typical type IV behavior with desorption hysteresis, which has micro and mesopores after pyrolysis. PPM rendered from PAN precursor showed nearly nonporous carbon behavior as shown in BET isotherm due to their low adsorbed volume and surface area.[23]

Pore size distribution of the five PPMs, shown in Figure 6, was calculated from the N_2 adsorption isotherm using the Barrett-Joyner-Halenda (BJH) method.[24] No significant difference in the average pore size of the PPMs was observed, except from the CA precursor. PPM from CA shows a mesoporous region between 3-5 nm.

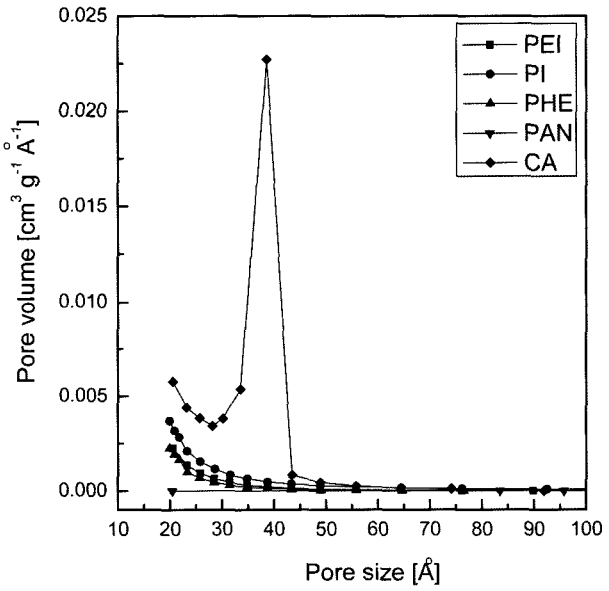

Figure 6. Pore size distribution of five pyrolyzed polymer membranes calculated by BJH method using the N_2 adsorption isotherm.

Surface area, pore volume, and average pore size of the five PPMs is summarized in Table III. The surface area of PPMs obtained after pyrolysis surpassed 400 m^2/g, except for PPM rendered from PAN. Originally, a thermal activation process in an aqueous H_2SO_4 solution[25] or oxidative stabilization process[17] is necessary for PAN to become a PPM precursor. Either process can make PPM more mechanically strong and resistant to high temperature processing, however, for a fair comparison of each PPM membrane, the thermal activation was not performed during PPM fabrication. For these reasons, PPM from PAN showed the smallest surface area and pore volume with a large pore size, which closely relates to the peculiar gas permeation and separation performance. This phenomenon will be explained in the next section.

Figure 7 shows the SEM images of a cross-section of each composite membrane. The PPM modules composed of two layers: selective and support. The selective layer or coated PPM, had an average thickness of 1-3 μm, except for the PHE precursor (5 μm). In order to compare the gas permeance of the PPMs, the coating layer thickness should be the same. However, because the main objective of this study is not to compare their permeation performance but to characterize the gas transport mechanism of PPM composite membrane modules, the effect of thickness was not considered in this study. Although the thickness of coating layer varied with external factors, gas transport mechanism through PPM membrane modules obtained from various polymeric precursors can be interpreted from the gas permeance data.

Gas Transport Property. Figure 8 shows the gas permeance of the five PPM membrane modules. From these results, gas permeation characteristics can be classified into two categories. Gas permeance of carbon membranes from PEI, PI and PHE was observed to be in the following order: $P(He) > P(CO_2) > P(O_2) > P(N_2)$, indicating that the permeability of small gas molecules (< 4 Å) through the microporous PPMs agree well with the order of the kinetic gas diameter. That is, trends in the gas permeation behavior follow the typical molecular sieving mechanism. PPM rendered from PI showed higher gas permeability than the other membranes. This can be inferred from the fact that the morphology of PI after pyrolysis might be suitable for creating microcavities. Among other polymer membranes, wholly

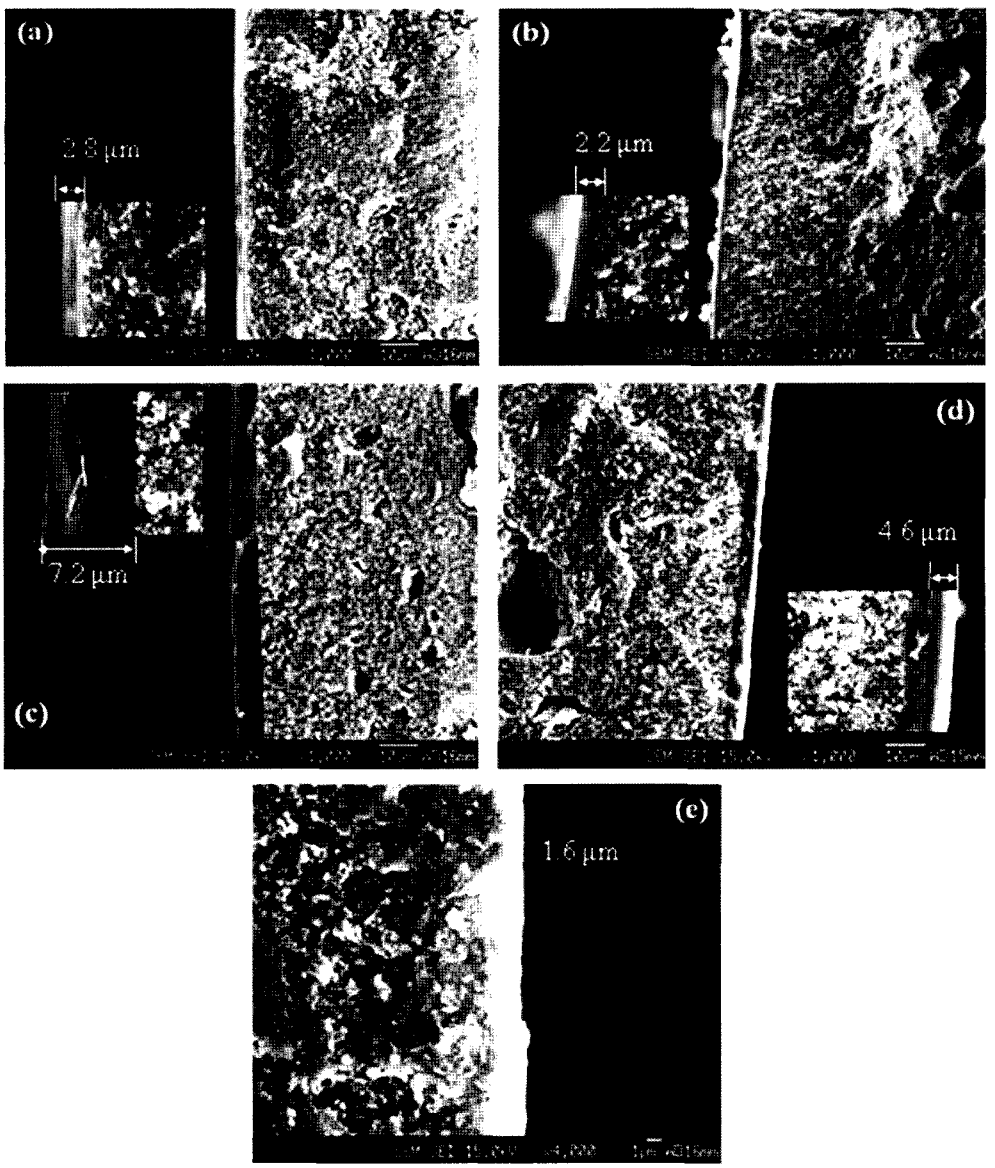

Figure 7. Field-emission scanning electron microscopy (FE-SEM) cross-sectional images of pyrolyzed polymer composite membrane rendered from (a) PEI, (b) PI, (c) PHE, (d) PAN, and (e) CA. Except for (e), images are 1000 × and 4000 ×.

aromatic PI having higher thermal stability can be helpful to reconstruct turbostratic amorphous carbon structure during mid-range pyrolysis. This might be the main reason for higher *d*-spacing value of PPM rendered from PI. High *d*-spacing and large pore volume obtained from BET analysis contributed to their high gas permeation characteristics. Alternatively, the gas permeances of PPMs from PAN and CA were different than those of PPMs from PEI, PI and PHE. Specifically, α (O_2/N_2) and α (CO_2/N_2) was close to one, as shown in Figure 9. To this end, Knudsen diffusion is the dominating mechanism for PPMs prepared from PAN and CA.

The separation factor is constant once the diffusion through a pore diameter is within Knudsen regime.[26] Generally, Knudsen diffusion is a significant transport and separation mechanism in porous membranes. When all other factors are equal, the ratio of the permeability of two gases, Q_A and Q_B, is the inverse square root of their molecular weight ratio:

$$Q_A/Q_B = (M_B/M_A)^{1/2} \quad (3)$$

where M_A and M_B is the molecular weight of A and B, respectively. To this end, Knudsen diffusion expresses the separation of gas molecules according to molecular weight. The gas separation is correlated with BET adsorption and desorption isotherm experiments, as shown in Table III. The pore diameter of PPMs from PAN and CA was larger than the other PPMs, resulting in the diffusion of small gases

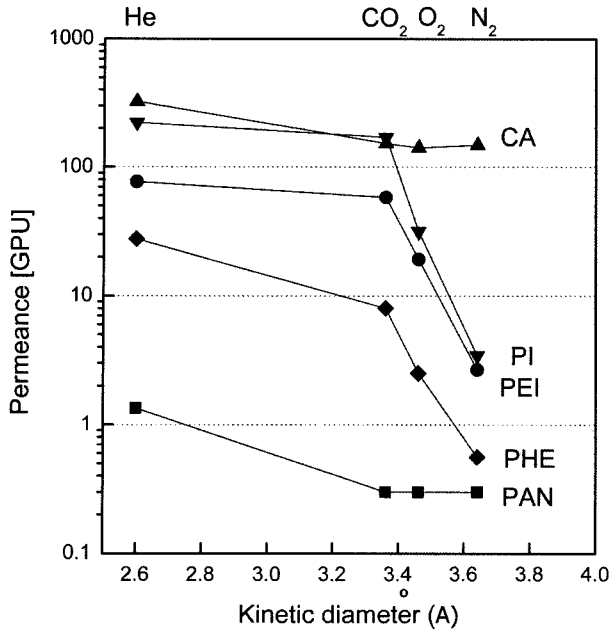

Figure 8. Single gas permeance of pyrolyzed membrane rendered from (a) PEI, (b) PI, (c) PHE, (d) PAN, and (e) CA.

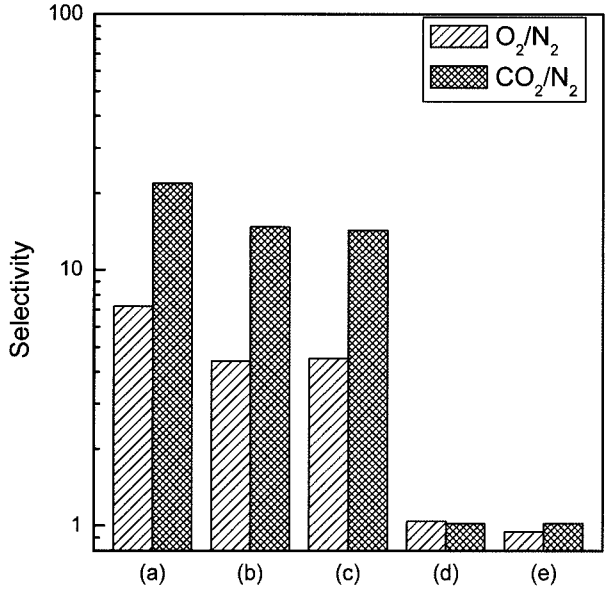

Figure 9. Permselectivity of pyrolyzed polymer composite membrane rendered from (a) PEI, (b) PI, (c) PHE, (d) PAN, and (e) CA.

through larger cavities (or pores). Additionally, the PAN pore volume was the lowest among all the PPM samples that is well coincided with the results on the smallest gas permeance for all tested gases. Specifically, the PPM prepared from PAN had a partial carbon membrane with an impermeable bulk structure and incomplete pore system as illustrated by the very small surface area and pore volume, and large pore size. Therefore, it is difficult for gases to permeate the membrane by solution diffusion or molecular sieving transport mechanism.[17] It should be noted that PAN did not undergo thermal oxidation process for activated pore creation.

Saufi and Ismail categorized the performance of PPMs for the separation of gas mixtures using flat sheets and composites.[4] Because gas permeance was tremendously varied with the coated layer thickness, comparison of different composite membrane module systems is impossible. However, permselectivities of PPM composite modules rendered from PI, PHE, and PAN reasonably matched with the study by Saufi and Ismail with similar pyrolysis conditions.

The effect of temperature on gas permeation is illustrated in an Arrhenius-type plot in Figure 10. The permeance of PEI, PI, and PHE increased with increasing temperature, with no significant loss of selectivity. As expected for the molecular sieving mechanism, gas transport was thermally activated. The apparent activation energy increased with the kinetic diameter of the gas molecules. As indicated by the negligible variation of helium permeance with temperature, the gas diffusion was not restricted by the small molecular size. However, for PAN and CA, the activation energy was negative (with exceptions of He, CO_2, O_2 for PAN and He for CA), indicating the permeability coefficients decrease with increasing temperature due to the weak size-sieving behavior of PAN and CA from Knudsen diffusion. Gilron and Soffer reported Knudsen diffusion in microporous carbon membranes having molecular sieving behavior. Specifically, the PPM experienced sieving behavior for larger molecules (d_m (kinetic gas diameter) > 0.43 nm) and Knudsen behavior for smaller molecules (d_m < 0.43 nm).[27] Thus, controlling the porosity of PPM by pyrolysis is an important factor in determining the gas separation mechanism and performance of a limited set of gas mixtures. The pore size distribution of PPM from PAN and CA was an intermediate of molecular sieving and Knudsen diffusion, and an optimum pore size may be controlled by an activation process, such as PDMS coating, to block the large pores.

Conclusions

In this study, the gas permeation performance characteristics of PPM modules rendered from five commercial polymeric precursors were compared. Dip-coating and pyrolysis conditions were selected according to the nature of the precursors and external variables, such as thermal stability, molecular weight, and solution viscosity. Additionally, a unique module design without organic sealant was adapted for easy replacement and reuse. Gas separation performance of the PPM modules indicated two distinctive trends in terms of selectivity. PPMs rendered from PI, PEI, and PHE showed typical molecular sieving mechanisms for all gases. However, PPMs from PAN and CA exhibited Knudsen dif-

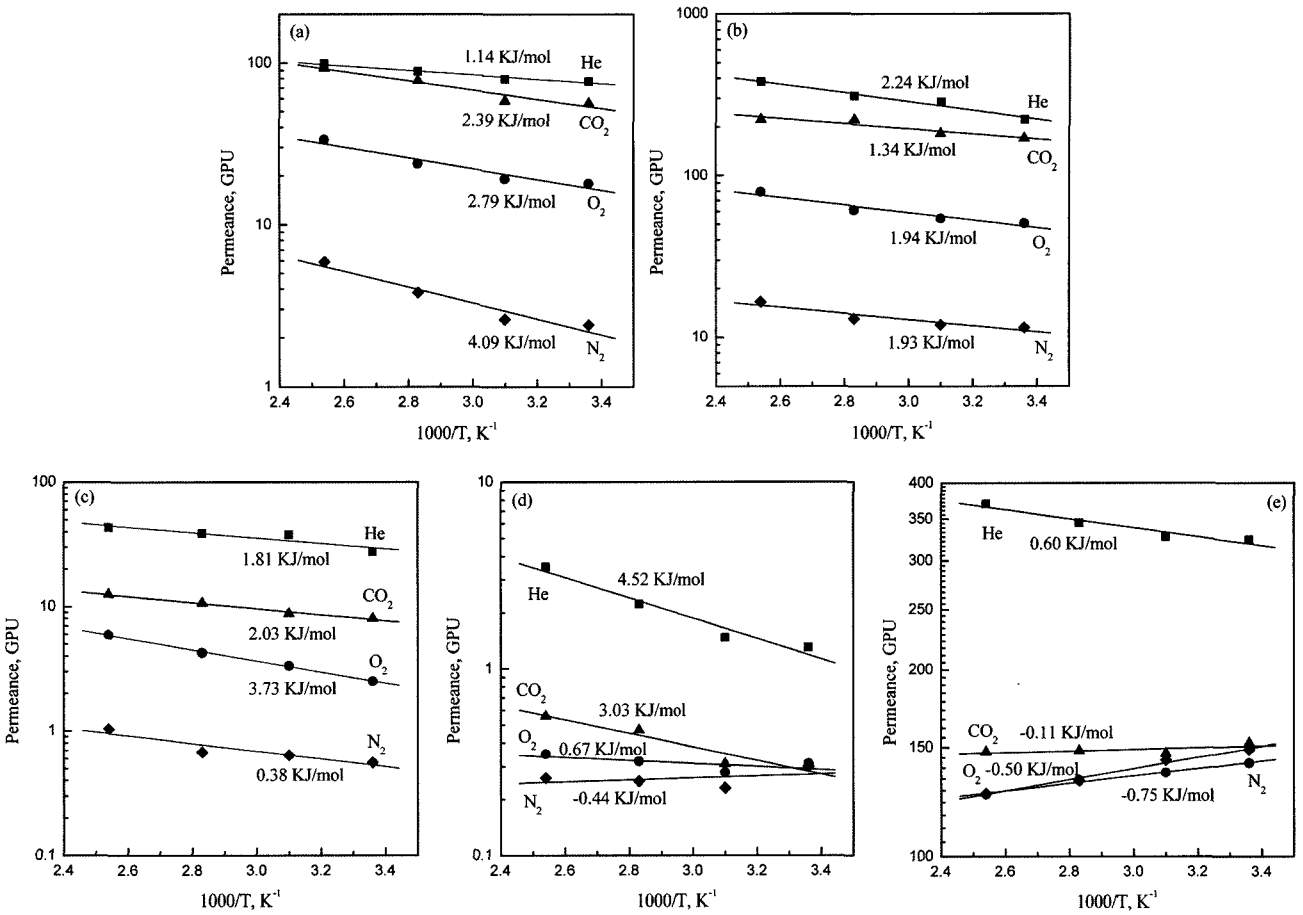

Figure 10. Effect of temperature on gas permeance of PPM. The indicated values correspond to apparent activation energies of (a) PEI, (b) PI, (c) PHE, (d) PAN, and (e) CA.

fusion with weak molecular sieving character for small gas molecules due to large pore size distribution. The Knudsen diffusion was confirmed by the negative temperature dependency of PPMs.

Acknowledgements. This research was supported by a grant (DB2-101) from Carbon Dioxide Reduction & Sequestration Research Center, one of the 21st Century Frontier programs funded by the Ministry of Science and Technology of Korean Government.

References

(1) M. Perez-Mendoza, *et al.*, *Carbon*, **44**, 638 (2006).
(2) D. Q. Vu, W. J. Koros, and S. J. Miller, *J. Membrane Sci.*, **211**, 311 (2003).
(3) H. Suda and K. Haraya, *Chem. Commun.*, 93 (1997).
(4) S. M. Saufi and A. F. Ismail, *Carbon*, **42**, 241 (2004).
(5) C. Liang, G. Sha, and S. Guo, *Carbon*, **37**, 1391 (1999).
(6) S. H. Park, *et al.*, *Macromol. Res.*, **11**, 157 (2003).
(7) H. Suda and K. Haraya, *J. Phys. Chem. B*, **101**, 3988 (1997).
(8) A. Singh-Ghosal and W. J. Koros, *J. Membrane Sci.*, **174**, 177 (2000).
(9) T. A. Centeno and A. B. Fuertes, *Sep. Purif. Technol.*, **25**, 379 (2001).
(10) T. A. Centeno, J. L. Vilas, and A. B. Fuertes, *J. Membrane Sci.*, **228**, 45 (2004).
(11) A. F. Ismail and L. I. B. David, *J. Membrane Sci.*, **193**, 1 (2001).
(12) W. Zhou, *et al.*, *J. Membrane Sci.*, **217**, 55 (2003).
(13) Y. K. Kim, H. B. Park, and Y. M. Lee, *J. Membrane Sci.*, **251**, 159 (2005).
(14) Y. K. Kim, H. B. Park, and Y. M. Lee, *J. Membrane Sci.*, **226**, 145 (2003).
(15) D.o.B.-R.L. Sadtler Research Laboratories *The Infrared Spectra Atlas of Monomers and Polymers*, 1984.
(16) R. K. Mariwala and H. C. Foley, *Ind. Eng. Chem. Res.*, **33**, 607 (1994).
(17) L. I. B. David and A. F. Ismail, *J. Membrane Sci.*, **213**, 285 (2003).
(18) H. M. Jeong, M. Y. Choi, and Y. T. Ahn, *Macromol. Res.*, **14**, 312 (2006).
(19) B. Grzyb, *et al.*, *J. Anal. Appl. Pyrol.*, **67**, 77 (2003).
(20) D. S. Kim, *et al.*, *Macromol. Res.*, **13**, 314 (2005).
(21) M. G. Sedigh, *et al.*, *Ind. Eng. Chem. Res.*, **38**, 3367 (1999).

(22) X. Zhang, *et al.*, *Sep. Purif. Technol.*, **52**, 261 (2006).
(23) D. K. Kim, *et al.*, *Macromol. Res.*, **13**, 521 (2005).
(24) E. P. Barrett, L. G. Joyner, and P. P. Halenda, *J. Am. Chem. Soc.*, **73**, 373 (1951).
(25) I. Mochida and S. Kawano, *Ind. Eng. Chem. Res.*, **30**, 2322 (1991).
(26) Jeffrey C. S. Wu, D. F. Flowers, and P. K. T. Liu, *J. Membrane Sci.*, **77**, 85 (1993).
(27) J. Gilron and A. Soffer, *J. Membrane Sci.*, **209**, 339 (2002).
(28) J. Hayashi, *et al.*, *Ind. Eng. Chem. Res.*, **34**, 4364 (1995).
(29) J. Hayashi, *et al.*, *Ind. Eng. Chem. Res.*, **35**, 4176 (1996).
(30) M. Yamaoto, *et al.*, *J. Membrane Sci.*, **133**, 195 (1997).
(31) A. Lapkin, *Membr. Tech.*, **116**, 5 (1999).
(32) W. Wei, *et al.*, *Carbon*, **40**, 465 (2002).
(33) W. Zhou, *et al.*, *Ind. Eng. Chem. Res.*, **40**, 4801 (2001).